

# Thermal Diffusivities of Small Molecule Organic Semiconductors: Inverted Anisotropy in Functionalized Acene Crystals

H. Zhang<sup>a</sup>, Y. Yao<sup>a</sup>, Marcia M. Payne<sup>b</sup>, Karl J. Thorley<sup>b</sup>, J.E. Anthony<sup>b</sup>, and J.W. Brill<sup>a</sup>

<sup>a</sup>Department of Physics and Astronomy, University of Kentucky, Lexington, KY 40506-0055

<sup>b</sup>Department of Chemistry, University of Kentucky, Lexington, KY 40506-005

**Abstract:** We have measured the interlayer and in-plane (needle axis) thermal diffusivities of 6,13-bis(triisopropylsilylethynyl) pentacene (TIPS-Pn). The needle axis value is comparable to the phonon thermal conductivities of quasi-one dimensional organic metals with excellent  $\pi$ -orbital overlap, and its value suggests that a significant fraction of heat is carried by optical phonons. Furthermore, the interlayer (**c**-axis) thermal diffusivity is at least an order of magnitude larger, and this unusual anisotropy implies very strong dispersion of optical modes in the interlayer direction, presumably due to interactions between the silyl-containing side groups. Similar values for both in-plane and interlayer diffusivities have been observed for several other functionalized acene semiconductors with related structures.

PACS: 66.70.-f, 81.05.Fb, 66.10.cd

## I. Introduction

Organic semiconducting materials are being studied for a variety of room temperature applications, especially where low-cost conformal materials that can be coated on complex structures are desired. Although most of the emphasis has been on studies of electronic and optical properties, it is also important to know thermal properties, in particular the thermal conductivities ( $\kappa$ ), for different functions. For example, for micron-channel thin-film transistors, e.g. to drive pixels in flexible displays, one requires a relatively large thermal conductivity to minimize Joule heating. For example, to keep heating less than  $\sim 10$  degrees, one needs  $\kappa > \kappa_0$ , where  $\kappa_0 \sim 10$  mW/cm $\cdot$ K [1]. On the other hand, low thermal conductivities, e.g.  $\kappa < \kappa_0$ , are needed for applications as room-temperature thermoelectric power generators. In such an embodiment, films of the polymer poly(3,4-ethylenedioxythiophene) (PEDOT) have thermal conductivity  $\kappa \sim 3$  mW/cm $\cdot$ K and films with  $\sim 20\%$  doping have room temperature thermoelectric figures of merit  $ZT \equiv S^2\sigma T/\kappa \sim 0.3-0.4$  [2,3] where  $S$  is the Seebeck coefficient,  $\sigma$  the electrical conductivity,  $T$  the temperature, and  $\kappa = \kappa_{el} + \kappa_{ph}$ , the sum of the electron and phonon thermal conductivities. While this value of  $ZT$  is smaller than the best inorganic thermoelectric materials (e.g. Bi<sub>2</sub>Te<sub>3</sub> has  $ZT \sim 1$  [4]), the lower material and processing costs make use of organic materials promising for specialized applications.

Because small molecule, crystalline organic semiconductors can have much higher charge carrier mobilities than polymers, they can be advantageous for some applications. For thermoelectric applications, for which the materials must be chemically doped to have sufficiently high conductivities, this will require that doping does not overly increase scattering due to disorder [5], e.g. substitutional doping with a molecule with a similar structure to the host. If this can be achieved, the higher mobility may allow lower-doping levels to be used, increasing the Seebeck coefficient. Since typically  $\kappa_{ph} > \kappa_{el}$ , relatively high values of  $ZT$  may be obtained if the phonon thermal conductivity is not much larger than that of polymers.

For example, pentacene is one of the best studied small molecule semiconductors, and films with 8% (by volume) doping have been measured to have  $S \sim 200$   $\mu$ V/K [6]. While pentacene is relatively insoluble and air sensitive, making processing costs expensive, a number of soluble acenes with functionalized side and end groups have been developed which have comparably high electronic mobilities [7]. For example, 6,13-bis(triisopropylsilylethynyl) (TIPS) pentacene [7-9] (see Figure 1a) films have been prepared with electronic mobilities  $\mu > 10$  cm<sup>2</sup>/V $\cdot$ s [10]. If 8% doped crystals can be prepared which maintain  $\mu \sim 10$  cm<sup>2</sup>/V $\cdot$ s, they would have  $\sigma \sim 160$  S/cm and  $\kappa_{el} \sim 1$  mW/cm $\cdot$ K (assuming the Wiedemann-Franz law), and if  $S \sim 200$   $\mu$ V/K and  $\kappa_{ph} \sim 4$  mW/cm $\cdot$ K, similar to rubrene [11,12], the thermoelectric figure of merit would be  $ZT \sim 0.4$ , comparable to the best polymers. Furthermore, improvements in sample quality and morphology may increase the mobility and  $ZT$ , because crystals with less doping may be used, keeping  $\sigma$  and  $\kappa$  the same but increasing  $S$ .

In this work, we discuss measurements of the room temperature thermal conductivities of TIPS-pentacene [7-10] and several other soluble, small molecule organic semiconductors with related structures, shown in Figure 1 [13-16]. Because these crystals are undoped, the electronic density is negligible and  $\kappa = \kappa_{ph}$ . All of these materials form layered crystals, with the acene (or substituted acene) backbones lying in the **ab**-plane, (where one hopes for good  $\pi$ -orbital overlap between molecules [7]) and the silyl or germyl side groups extend between layers [7-9, 13-16]. The interlayer (**c**-axis) and in-plane phonon thermal conductivities are expected to be different,

so we endeavored to measure them separately. Because the available crystals are small (in-plane dimensions typically 0.5-10 mm and interlayer direction less than 0.5 mm), these could not be measured by conventional dc-techniques, and we used ac-calorimetry techniques [12,17], which yield the thermal diffusivity,  $D \equiv \kappa/c\rho$ , where  $c$  is the specific heat and  $\rho$  the mass density.

## II. Methods and Materials

The inter-layer measurement technique is described in detail in Ref. [12]. Light, chopped at frequency  $\omega$ , illuminates the top surface of the sample, with area  $A$  and uniform thickness  $d$ , and the temperature oscillations on the bottom surface are measured with a flattened, 25  $\mu\text{m}$  diameter chromel-constantan thermocouple glued to the surface with silver paint [12,19]. The oscillating thermocouple signal,  $V_\omega$ , is measured with a 2-phase lock-in amplifier with a transformer input. If the chopping period is much less than the time constant with which the sample comes to equilibrium with the bath ( $\tau_1 \gg 1$  s for our samples), the temperature oscillations of the bottom of the sample are given by

$$T_\omega = 2P_0A\Phi(\omega)/(\pi\omega C) \quad (1a)$$

$$\text{with } \Phi(\omega) = \sqrt{2}\chi/[\sinh^2\chi \cos^2\chi + \cosh^2\chi \sin^2\chi]^{1/2} \approx [1 + (\omega\tau_2)^2]^{-1/2}. \quad (1b)$$

Here  $P_0$  is the intensity of the light,  $C$  the sample heat capacity,  $\chi \equiv [\sqrt{90} \omega\tau_2/2]^{1/2}$ , and  $\tau_2$  the internal thermal time constant describing heat flow through the thickness of the sample (i.e. along the  $c$ -axis for our samples):

$$\tau_2 \equiv d^2/\sqrt{90}D_c \quad (2)$$

where  $D_c = \kappa_c/c\rho$  is the transverse, interlayer thermal diffusivity [12,18].

As discussed in Ref. [12], however, one also needs to consider the time response of the thermometer, which for our technique is dominated by the interface thermal resistance between the silver paint and sample. On test materials, we measured room temperature values of the interface time constant ( $\tau_{\text{ifc}}$ ) between 1-10 ms, depending on the material [12], for silver paint contact areas  $\sim 1 \text{ mm}^2$ . (Because the materials studied here are slightly soluble in the butyl acetate base of the paint, the interface time constant was expected to be closer to 1 ms.) If sample cooling is predominantly by surrounding gas and/or radiation, as is generally the case for these samples, the resulting measured time constant (so that  $\omega T_\omega \sim [1 + (\omega\tau_{\text{meas}})^2]^{-1/2}$ ) is  $\tau_{\text{meas}} \approx (\tau_2^2 + \tau_{\text{ifc}}^2)^{1/2}$ , whereas if heat primarily leaves the sample through the thermometer leads, then  $\tau_{\text{meas}} \approx \tau_2 + \tau_{\text{ifc}}$ , (as assumed for our measurements on rubrene [12]). In either case, if  $\tau_{\text{meas}}$  is a few ms, we cannot assume that the effects of the interface thermal resistance are small, and we can only find a lower limit for  $D_c$ , i.e.  $D_c > d^2/\sqrt{90}\tau_{\text{meas}}$ .

In fact, as discussed below, all the samples discussed in this paper had unexpectedly fast responses, with  $\tau_{\text{meas}} < 4$  ms. To be sure that we were not measuring spurious electronic signals at high frequencies, the lock-in amplifier was operated in X-Y mode and the frequency dependence of the “offset” signal, measured with the light off was subtracted from the “light-on” signal [12]. Also, to eliminate signals from unwanted heating of the thermocouple wires

away from the sample, we masked these from the light in different ways and found that the masks did not affect the measured thermocouple voltages.

For longitudinal, in-plane thermal conductivity ( $\kappa_{\text{long}}$ ) measurements, we use the technique of Hatta, *etal* [17]. A movable screen is placed between the chopped light source and sample, and the temperature oscillations are measured (with a thermocouple again glued to the sample with silver paint) on the back side of the sample in the screened portion. If  $\omega\tau_2 \ll 1$ , the position dependence of the oscillating temperature is given by [17]:

$$d\ln T_{\omega}(x) / dx = - (\omega/2D_{\text{long}})^{1/2} \quad (3)$$

where  $D_{\text{long}} = \kappa_{\text{long}}/c\rho$  and  $x$  = the distance between the thermometer and edge of the screen. In our setup, the screen is attached to a micrometer (precision  $\pm 3 \mu\text{m}$ ) which measures the distance,  $x_0 - x$ , where the offset  $x_0$  depends on the relative positions of the sample and screen. For these measurements, the frequency is fixed so that the thermal response of the thermometer does not enter. To be sure that we are in the correct frequency limit and the edge of the screen is not too close to the thermometer (i.e. overlapping with the silver paint spot) we check that we obtain the same values for the “frequency normalized” slopes,  $\omega^{-1/2} d\ln T_{\omega}/dx$  at different frequencies, as shown in Figure 2, below. Because Eqn. (3) assumes that both the illuminated and screened portions of the sample are much longer than the longitudinal diffusion length,  $(D_{\text{long}}/\omega)^{1/2}$ , which is typically  $\sim 0.5$  mm for our samples and frequencies, data was taken on needle shaped samples  $\sim 1$  cm long

Note that for both techniques, it is necessary that the sample is uniformly illuminated on a length scale much greater than the smaller of the longitudinal diffusion length or longitudinal dimensions of the sample. Visible/NIR light from a quartz-halogen lamp is transmitted to the sample through a glass light pipe and illuminates the sample, in vacuum, through an appropriate lens [12,19] giving a typical dc-temperature rise of the sample of a few degrees. It is also necessary that the light is mostly absorbed at its front surface. Although most samples were considered sufficiently opaque, in some cases, a light absorbing PbS film was evaporated on the top surface of the sample [12,19] and the experiment repeated; the PbS film was observed to not change the measured frequency dependence.

The molecular structures of the crystals investigated are shown in Figure 1. As mentioned above, all of these have layered crystal structures, with layers normal to  $c$  and the silyl or germlyl side groups extended, at an angle, between layers. TIPS-pn [7-10], F<sub>8</sub>-TIPS-pn [13], F<sub>2</sub>-TIPS-pn [16], and CP-DIPS-Pn [16] all have similar brick-layer structures in the plane. Crystals are typically needles, up to  $\sim 1$  cm in length, with the needle direction along  $[2, 1, 0]$  (as referenced to the TIPS-Pn unit cell), the direction of best  $\pi$ -orbital overlap [7-9]. Because the cyclopropyl group makes the side groups slightly more rigid in CP-DIPS-Pn than in the other crystals (e.g. as measured by thermal ellipsoids), the molecules are more tightly packed; e.g. the unit cell of CP-DIPS-pn is 6% smaller than that of TIPS-pn [16]. (Table 1 lists the molecular volumes, i.e. unit cell volume/number of molecules per cell.) For TIPS-Pn and F<sub>2</sub>-TIPS-Pn, the needles could be thicker than 250  $\mu\text{m}$ , but usable needles of F<sub>8</sub>-TIPS-Pn and CP-DIPS-Pn were  $< 100 \mu\text{m}$  thick and had very short time constants ( $\tau_{\text{meas}} < 1.5$  ms). Therefore, meaningful transverse measurements could not be made and only results for  $D_{\text{long}}$  are presented for these two materials.

TIPGe-Pn, EtTP-5, and TIPS-tetracene crystals grow as thick ( $d > 200 \mu\text{m}$ ) flakes (in plane dimensions  $< 3$  mm), so these were only used for  $D_{\text{trans}}$  measurements. Molecules in EtTP-5 are coplanar (along  $[010]$ ) but far apart ( $\sim 10 \text{ \AA}$ ), so there is very poor  $\pi$ -orbital overlap [15]. In

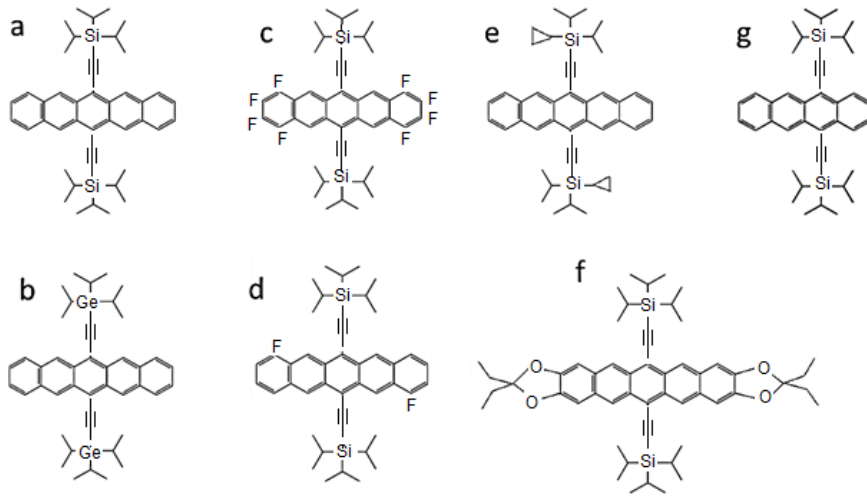


**Figure 1.** Molecular structures of crystals studied:

- a) bis(triisopropylsilylethynyl) pentacene (TIPS-Pn [7-9]);
- b) bis(triisopropylgermylethynyl) pentacene (TIPGe-Pn) [16];
- c) bis(triisopropylsilylethynyl) octafluoropentacene ( $F_8$ -TIPS-Pn [13]);
- d) bis(triisopropylsilylethynyl) perfluoropentacene ( $F_2$ -TIPS-Pn[16]);
- e) bis(cyclopropyl-diisopropylsilylethynyl) pentacene (CP-DIPS-Pn [16]);
- f) tetraethyl-bis(triisopropylsilylethynyl)-tetraoxadicyclopenta[b,m] pentacene (EtTP-5 [15]);
- g) bis(triisopropylsilylethynyl) tetracene (TIPS-tetracene [14]).

TIPS-tetracene [14] and TIPGe-Pn [16], the orientation of the acene backbones alternate in the **ab**-plane, so there is also poor  $\pi$ -orbital overlap. While these materials would therefore not be useful for electronic applications, we studied them to help understand thermal transport in this class of materials.

### III. Results and Discussion

In Figure 2, we plot  $f^{1/2} \ln V_\omega$  as a function of position behind a screen, where  $f \equiv \omega/2\pi$  is the chopping frequency for a TIPS-pn crystal at a few frequencies. From Eqtn. (3), the slope is inversely proportional to  $D_{\text{long}}^{1/2}$ . For large  $x$ , the edge of the screen is overlapping with the silver paint holding the thermocouple, and the signal begins to saturate, whereas for small  $x$ , the edge of the screen is far from the thermocouple so  $V_\omega$  is small and approaching the thermocouple offset voltage and noise level. For intermediate distances, the same slope,  $f^{1/2} d \ln V_\omega / dx$ , is measured for different frequencies, yielding  $D_{\text{long}} = 1.0 \pm 0.1 \text{ mm}^2/\text{s}$ . (Similar values were found

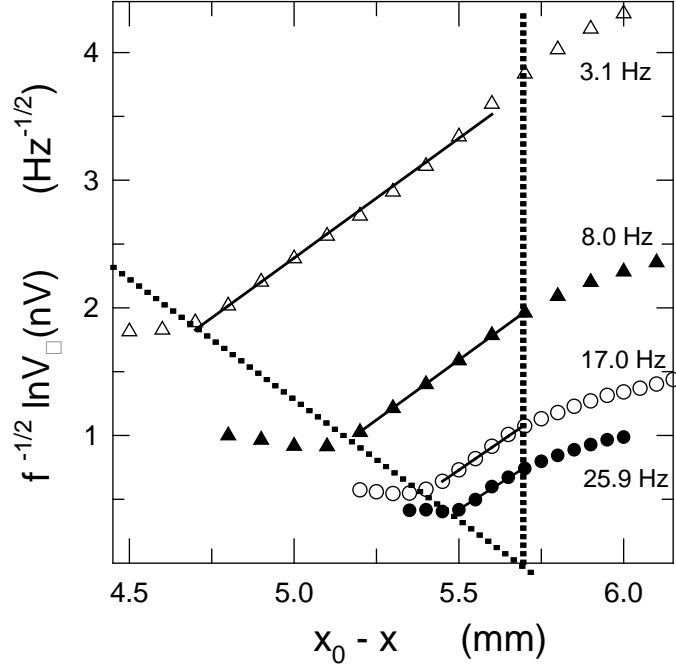


**Figure 2.** Spatial dependence of  $V_\omega$  for an 8 mm long TIPS-Pn crystal at several frequencies. The dotted lines outline the region of linear variation of  $\ln(V_\omega)$ , shown by the solid lines, where the slope of  $f^{-1/2} \ln(V_\omega)$  is expected to be independent of frequency. On the right of the dotted lines, the signal begins to saturate as the illuminated portion of the sample overlaps with the

for other crystals.) The specific heat of TIPS-pn, measured on a pellet with differential scanning calorimetry with a precision  $\sim 3\%$  [20], is shown in the Figure 3 inset. Using  $c = 1.48 \text{ J/gK}$  and density  $\rho = 1.1 \text{ g/cm}^3$  [7], we find  $\kappa_{\text{long}} = 16 \pm 2 \text{ mW/cm}\cdot\text{K}$ .

This value of  $\kappa_{\text{long}}$  is several times larger than the room temperature value for rubrene [11], but comparable to the phonon thermal conductivity of quasi-one dimensional organic conductors containing segregated stacks or organic molecules with excellent  $\pi$ -orbital overlap [21-23]. In fact, its value suggests that, in addition to acoustic phonons, a significant fraction of the heat is carried by low energy, propagating optical phonons. The room temperature specific heat is over thirty times the value associated with acoustic modes ( $c_{\text{acoustic}} = 3R/M = 0.039 \text{ J/g}\cdot\text{K}$ , where  $R$  is the gas constant and the molecular weight  $M = 638 \text{ g/mole}$ ), indicating that most of the room temperature specific heat is due to excitation of optical modes. (The room temperature specific heat is also only  $\sim 1/3$  of its Dulong-Petit value, indicating that the majority of optical modes are not yet excited, having energies  $> 200 \text{ cm}^{-1} \sim \text{room temperature}$ .) Consider

$$\kappa = (\rho/3)\sum c_j v_j \lambda_j, \quad (4)$$

where  $c_j$ ,  $v_j$ , and  $\lambda_j$  are the specific heat, propagation velocity, and mean-free path associated with phonons of mode  $j$ . If the acoustic modes have velocities between 1 and 3 km/s (typical for molecular solids [24] and we assume that only the acoustic modes are propagating, Eqtn. (4)

implies that  $\lambda > 400 \text{ \AA}$ , i.e.  $> 50$  in-plane lattice constants. While this is not impossible, it is much larger than expected for molecular solids, where acoustic modes are expected to have significant scattering from molecular librations of the isopropyl side groups. In addition, it has been shown that there is large thermal motion of the TIPS-pn molecule along the long-axis of the pentacene backbone [25], which should also decrease the mean-free path of acoustic phonons propagating along the needle axis. If the mean-free paths are in fact relatively small, much of the heat must be carried by sufficiently dispersive optical modes.

Figure 3 shows the frequency dependence of  $fV_\omega$  for four crystals of TIPS-pn of different thicknesses, with their resulting values of  $\tau_{\text{meas}}$ . In fact, we started with measurements on thin crystals, as we expected low values for  $D_c$  as we had observed for rubrene [12], but in fact  $\tau_{\text{meas}} > 1 \text{ ms}$  for all crystals. Since this value is comparable to the expected value for  $\tau_{\text{ifc}}$  (e.g., for rubrene, we found  $\tau_{\text{ifc}} < 6 \text{ ms}$  [12]), and because we observe no correlation of  $\tau_{\text{meas}}$  with thickness, we assume that we are limited by the resistance of the thermal interface between the sample and silver paint.

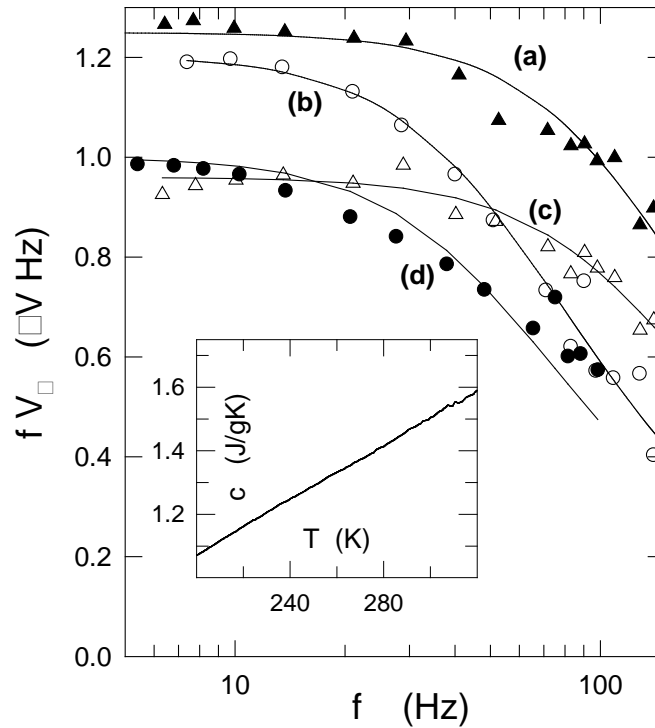


**Figure 3.** Frequency dependence of  $fV_\omega$  for four TIPS-pentacene crystals, with their fits to  $fV_\omega = \text{constant}/[1+(\omega\tau_{\text{meas}})^2]^{1/2}$ : a)  $d = 335 \text{ }\mu\text{m}$ ,  $\tau_{\text{meas}} = 1.3 \text{ ms}$ ; b)  $d = 610 \text{ }\mu\text{m}$ ,  $\tau_{\text{meas}} = 2.8 \text{ ms}$ ; c)  $d = 215 \text{ }\mu\text{m}$ ,  $\tau_{\text{meas}} = 1.2 \text{ ms}$ ; d)  $d \approx 100 \text{ }\mu\text{m}$ ,  $\tau_{\text{meas}} \approx 3 \text{ ms}$  (signal  $\div 6$ ). The noise in  $fV_\omega$  is indicated by the scatter in the data. Inset: Specific heat of a TIPS-Pn pellet measured with differential scanning calorimetry.

We note from Eqtn. (1) that  $fV_\omega$  can be frequency-independent not only if  $D$  is large but also if  $D$  is proportional to frequency, i.e.  $c \propto 1/\omega$ . Frequency dependent specific heats are known at glass transitions [29], and one might guess that as the butyl acetate solvent of the silver paint dries, it leaves the TIPS-Pn in a glassy state. However, this cannot explain our results; if there is a glassy interface with a frequency-dependent specific heat or thermal resistance, it is still in series with the bulk of the sample through which heat must diffuse. (However, a frequency-dependent interface resistance may explain some behavior at lower frequencies, discussed later.) Alternatively, one might suppose that the glassy region penetrates most of the sample, so that the “normal” region is negligible. This seems extremely unlikely for our thick samples; e.g. no change in size or shape of the samples is observed. In addition, TIPS-Pn easily recrystallizes from butyl acetate solvents, suggesting that the crystalline nature of the material will not be excessively disturbed by the use of this solvent. Furthermore,  $c \propto 1/\omega$  is a much stronger frequency dependence of the specific heat than observed at glass transitions, where a large fraction of the specific heat is frequency independent [29].

Thus we assume that the intrinsic  $\tau_2$  of the sample is less than  $\tau_{\text{meas}}$ , which therefore sets a lower limit for the interlayer diffusivity; from the 610  $\mu\text{m}$  sample, we find  $D_c > 14 \text{ mm}^2/\text{s}$  and  $\kappa_c > 225 \text{ mW}/\text{cm}^2 \cdot \text{K}$ . These values are much larger than typically found in a van-der-Waals bonded molecular crystal (e.g. for rubrene we measured  $D_c \sim 0.05 \text{ mm}^2/\text{s}$ , giving  $\kappa_c \sim 0.7$  [12], while for pentacene  $\kappa_c = 5.1 \text{ mW}/\text{cm}^2 \cdot \text{K}$  [26]), and are comparable to the values for materials with extended bonding (e.g.  $\text{Al}_2\text{O}_3$  has  $D \sim 10 \text{ mm}^2/\text{s}$  and  $\kappa \sim 300 \text{ mW}/\text{cm} \cdot \text{K}$  [27]). Also surprising is the anisotropy,  $\kappa_c > 14 \kappa_{\text{long}}$ ; because the in-plane bonding was assumed to be stronger than the inter-plane bonding, we expected the longitudinal thermal conductivity to be greater than the transverse. (This expected anisotropy was observed for rubrene:  $\kappa_c \sim \kappa_{\text{long}}/6$  [12].) If one assumes that thermal transport is dominated by intermolecular thermal resistances and these were *equal* for *c*-axis and in-plane bonds, then the thermal conductivities in different directions would be proportional to the packing densities in their transverse planes [28], but this could only account for only a factor of  $\sim 2$  in thermal anisotropy because  $a \sim b \sim c/2$  [7]. Therefore, we must conclude that there must be stronger phonon interactions between the side groups than between the pentacene backbones, giving rise to more dispersion of optical phonons and therefore a larger amount of heat carried by optical modes along *c* than in the plane. (If instead, one assumes that all of the heat is carried by acoustic phonons, then the same analysis used for  $\kappa_{\text{long}}$  would give an interlayer phonon mean-free-path  $\lambda_c > 300 \text{ c}$ !)

To check these results for TIPS-Pn, we measured the transverse and longitudinal diffusivities of several related materials, listed in Figure 1. Figure 4 shows representative spatial dependences of  $\ln(V_\omega)$  for crystals of CP-TIPS-Pn,  $\text{F}_2$ -TIPS-Pn, and  $\text{F}_8$ -TIPS-Pn. The measured slopes and calculated longitudinal diffusivities are listed in Table 1. As discussed above, slopes were measured at a few frequencies for each crystal and the uncertainties given in the table reflect the variations in slopes. The fluorinated crystals may have slightly steeper slopes, and therefore lower thermal diffusivities, than TIPS-Pn, but the differences are less than the uncertainties in the measurement. The slopes for CP-TIPS-Pn had more scatter, probably reflecting the somewhat shorter crystals available, but were always considerably steeper than for the other compounds, as shown in the figure and table. The resulting lower diffusivity for CP-TIPS-Pn is surprising because one would expect the more rigid side-groups to reduce scattering of acoustic phonons. It again suggests that much of the heat is carried by molecular vibrations, and that the greater rigidity of the side-groups reduces the dispersion of the relevant, low-energy

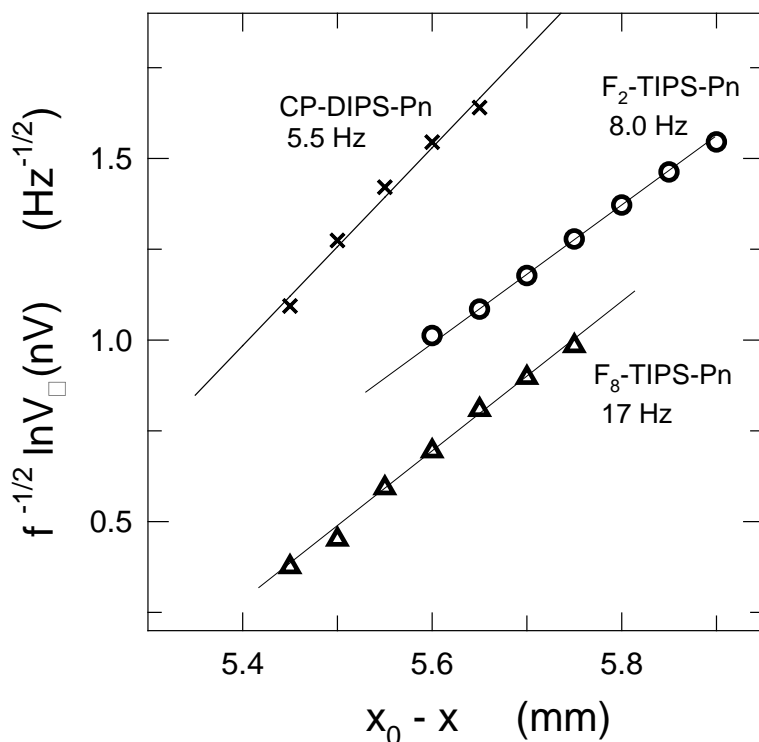


**Figure 4.** Spatial dependence of  $V_\omega$  for crystals of CP-DIPS-Pn (length = 6 mm),  $F_2$ -TIPS-Pn (length = 10 mm), and  $F_8$ -TIPS-Pn (length = 11 mm) at selected frequencies in their expected linear regions. The lines are guides to the eye. Note that the position offset,  $x_0$ , is different for each crystal.

Material	Molecular Volume ( $\text{nm}^3$ )	$-f^{-1/2} \frac{d \ln V_\omega}{dx}$ ( $\text{Hz}^{1/2} \cdot \text{mm}^{-1}$ )	$D_{\text{long}}$ ( $\text{mm}^2/\text{s}$ )	$d$ ( $\mu\text{m}$ )	$\tau_{\text{meas}}$ (ms)	$D_c$ ( $\text{mm}^2/\text{s}$ )
TIPS-Pn [7]	0.96	$1.77 \pm 0.06$	$1.00 \pm 0.10$	610	2.8	$> 14$
$F_2$ -TIPS-Pn [16]	0.94	$1.89 \pm 0.07$	$0.88 \pm 0.09$	300	1.26	$> 7$
$F_8$ -TIPS-Pn [13]	0.99	$1.98 \pm 0.10$	$0.80 \pm 0.10$	---	---	---
CP-DIPS-Pn [16]	0.90	$2.7 \pm 0.3$	$0.43 \pm 0.10$	---	---	---
TIPGe-Pn [16]	0.96	---	---	460	1.1	$> 20$
EtTP-5 [15]	1.02	---	---	300	0.68	$> 14$
TIPS-tetracene [14]	0.91	---	---	290	$< 0.4$	$> 20$

**Table 1.** Molecular volumes, slopes and  $D_{\text{long}}$  (from position dependent measurements), and thicknesses, measured time constants, and lower-limits for  $D_c$  (from frequency dependent measurements).

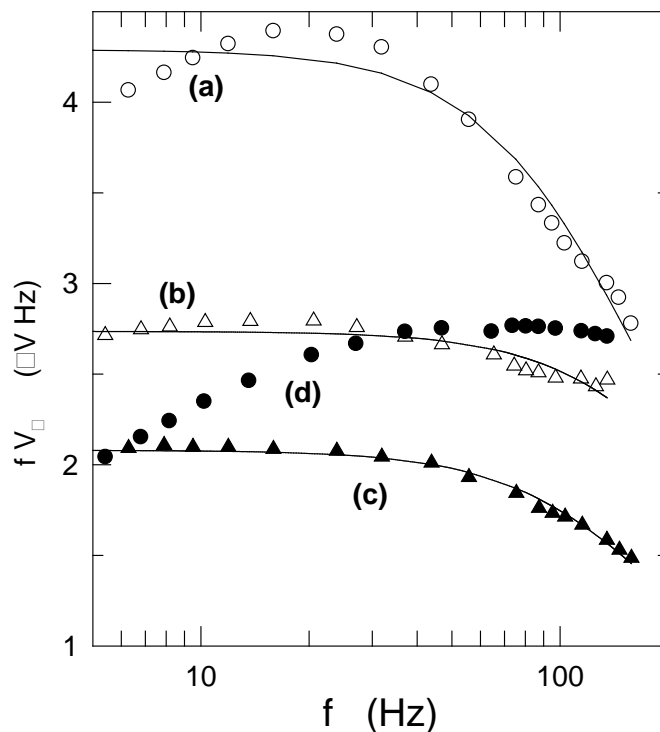


**Figure 5.** Frequency dependence of  $fV_\omega$ , with fits to  $fV_\omega = \text{constant}/[1+(\omega\tau_{\text{meas}})^2]^{1/2}$ , for representative crystals of a)  $F_2$ -TIPS-Pn ( $d \approx 300 \mu\text{m}$ ,  $\tau_{\text{meas}} = 1.26 \text{ ms}$ ); b) EtTP-5 ( $d \approx 300 \mu\text{m}$ ,  $\tau_{\text{meas}} = 0.68 \text{ ms}$ ); c) TIPGe-Pn  $d = 460 \mu\text{m}$ ,  $\tau_{\text{meas}} = 1.03 \text{ ms}$  (signal  $\times 2$ ); d) TIPS-tetracene ( $d = 290 \mu\text{m}$ ). No fit is shown for TIPS-tetracene because of its strong, anomalous low frequency dependence, discussed in the text. The noise in  $fV_\omega$  is indicated by the scatter in the data.

( $\leq kT$ ) optical modes. Unfortunately, we have been unable to obtain meaningful data for the transverse diffusivity of CP-TIPS-Pn.

Figure 5 shows the frequency dependence of  $fV_\omega$  for several crystals; the thicknesses and values of  $\tau_{\text{meas}}$  are shown in the figure and listed in Table 1. In all cases,  $\tau_{\text{meas}}$  was too short for us to assume that the interface thermal resistance is negligible so we again only find lower limits for  $D_c$ . (In all cases, a few crystals were measured; the figure and table show representative cases.) As for TIPS-Pn, the transverse diffusivities are much larger than generally found for van-der-Waals bonded molecular crystals suggesting that, in all these materials, most of the transverse heat conduction is by propagating optical phonons implying strong interactions between molecular vibrations, presumably of the side groups. It is noteworthy that this is even true for EtTP-5, TIPGe-Pn, and TIPS-tetracene, with poor  $\pi$ -orbital overlap in the plane.

As shown in Figure 5,  $F_2$ -TIPS-Pn and TIPS-tetracene crystals also exhibit anomalous decreases in  $fV_\omega$  at low frequencies. This frequency dependence superficially resembles what is expected for frequencies near and below  $1/\tau_1$ , the external thermal time constant, but for these samples  $\tau_1 \gg 1$  second. Low frequency decreases have also been observed for some other samples measured, such as TIPS-Pn sample (c) in Figure 3 and have also been seen by us in

other materials in the past [19]. We are not sure of the cause, but one possibility is that the interface thermal resistance decreases with increasing frequency. As discussed above, since the interface resistance is in series with the sample's thermal resistance, this effect does not change our conclusion about the large value of  $D_c$  determined from higher frequencies for these materials.

The large thermal diffusivities indicate that, for those of these materials with brick-layer structures and high electronic mobility, Joule heating of micro-electronic components should not be a problem. While the longitudinal diffusivities are slightly larger than desired for thermoelectric applications, they are not excessive. However, thermoelectric devices would need to be constructed so that the very high transverse diffusivities do not create thermal shunts. Furthermore, thermal conductivities of thin films, probably relevant for most applications, may be smaller than bulk values due to interface phonon scattering.

In summary, we have measured the longitudinal (needle-axis) and transverse, interlayer thermal conductivities of crystals of TIPS-Pn by ac-calorimetry. We have found that the longitudinal value is higher than that of rubrene [11] and pentacene [26] and comparable to quasi-one dimensional conductors with excellent  $\pi$ -orbital overlap [21-23]. The transverse thermal diffusivity is at least an order of magnitude *larger* than the longitudinal. These values and inverted anisotropy of  $\kappa$  indicate that molecular vibrations, presumably concentrated on the silyl-containing side groups, have sufficient intermolecular interactions and dispersion to carry most of the heat. Similar values for both the in-plane and interlayer thermal diffusivities were found for several other materials with related structures.

This research was supported in part by the National Science Foundation, grant DMR-1262261. The synthesis and crystal engineering of organic semiconductors was supported by the Office of Naval Research, grant N00014-11-1-0328.

## References

- [1] L. Maiolo, M. Cuscuna, L. Mariucci, A. Minotti, A. Pecora, D. Simeone, A. Valeeta, and G. Fortunato, Analysis of self-heating related instability in n-channel polysilicon thin film transistors fabricated on polyimide, *Thin Solid Films* **517**, 6371 (2009).
- [2] O. Bubnova, Z.U. Khan, A. Malti, S. Braun, M. Fahlman, M. Berggren, and X. Crispin, Optimization of the thermoelectric figure of merit in the conducting polymer poly(3,4-ethylenedioxythiophene), *Nature Materials* **10**, 429 (2011).
- [3] G.-H. Kim, L. Shao, K. Zhang, and K.P. Pipe, Engineered doping of organic semiconductors for enhanced thermoelectric efficiency, *Nature Materials* **12**, 719 (2013).
- [4] T.M. Tritt, Thermoelectric Phenomena , Materials, and Applications, *Annu. Rev. Mater. Res.* **41**, 433 (2011).

- [5] K. Harada, M. Sumino, C. Adachi, S. Tanaka, and K. Miyazaki, Improved thermoelectric performance of organic thin-film elements utilizing a bilayer of pentacene and 2,3,5,6-tetrafluoro-7,7,8,8-tetracyanoquinodimethane (F<sub>4</sub>-TCNQ), *Appl. Phys. Lett.* **96**, 253304 (2010).
- [6] G.-H. Kim, M. Shtein, and K.P. Pipe, Thermoelectric and bulk mobility measurements in pentacene thin films, *Appl. Phys. Lett.* **98**, 093393 (2011).
- [7] J.E. Anthony, Functionalized Acenes and Heteroacenes for Organic Electronics, *Chem. Rev.* **106**, 5028 (2006).
- [8] J.E. Anthony, J.S. Brooks, D.L. Eaton, and S.R. Parkin, Functionalized pentacene: Improved electronic properties from control of solid-state order, *J. Am. Chem. Soc.* **123**, 9482 (2001).
- [9] J. Chen, D.C. Martin, and J.E. Anthony, Morphology and molecular orientation of thin-film bis(triisopropylsilylethynyl) pentacene, *J. Mater. Res.* **22**, 1701 (2007).
- [10] Y. Diao, B. C.-K. Tee, G. Giri, J. Xu, D.H. Kim, H.A. Becerril, R.M. Stoltenberg, T.H. Lee, G. Xue, S.C. Mannsfeld, and Z. Bao, Solution coating of large-area organic semiconductor thin films with aligned-crystalline domains, *Nature Materials* **12**, 665 (2013).
- [11] Y. Okada, M. Uno, Y. Nakazawa, K. Sasai, K. Matsukawa, M. Yoshimura, Y. Kitaoka, Y. Mori, and J. Takeya, Low-temperature thermal conductivity of bulk and film-like rubrene single crystals, *Phys. Rev. B* **83**, 113305 (2011).
- [12] H. Zhang and J.W. Brill, Interlayer thermal conductivity of rubrene measured by ac-calorimetry, *J. Appl. Phys.* **114**, 043508 (2013).
- [13] C. R. Swartz, S. R. Parkin, J. E. Bullock, J. E. Anthony, A. C. Mayer, G. G. Malliaras, Synthesis and characterization of electron-deficient pentacenes, *Org. Lett.* **7**, 3163 (2005).
- [14] S. A. Odom, S. R. Parkin, J. E. Anthony, Tetracene derivatives as potential red emitters for organic LEDs, *Org. Lett.* **5**, 4245-4248 (2003)
- [15] M. A. Wolak, J. Delcamp, C. A. Landis, P. A. Lane, J. Anthony, Z. H. Kafafi, "High performance organic light-emitting diodes based on dioxolane-substituted pentacene derivatives" *Adv. Func. Mater.* **16**, 1943 (2006)
- [16] S.R. Parkin and J.E. Anthony, private communication.
- [17] I. Hatta, Y. Sasuga, R. Kato, A. Maesono, Thermal diffusivity measurement of thin films by means of an ac calorimetric method, *Rev. Sci. Inst.* **56**, 1643 (1985).
- [18] P.F. Sullivan and G. Seidel, Steady-State ac-Calorimetry, *Phys. Rev.* **173**, 679 (1968).

- [19] M. Chung, E. Figueroa, Y.-K. Kuo, Yiqin Wang, J.W. Brill, T. Burgin, and L.K. Montgomery, Thermodynamics of the anion ordering transitions in  $(\text{TMTSF})_2\text{ReO}_4$  and  $(\text{TMTSF})_2\text{BF}_4$ , *Phys. Rev. B* **48**, 9256 (1993).
- [20] Yiqin Wang, M. Chung, T.N. O’Neal, and J.W. Brill, Differential scanning calorimetry at charge-density-wave transitions, *Synth. Met.* **46**, 307 (1992).
- [21] M.B. Salamon, J.W. bray, G. DePasquali, R.A. Craven, G. Stucky, and A. Schultz, Thermal conductivity of tetrathiafulvalene-tetracyanoquinodimethane (TTF-TCNQ) near the metal-insulator transition, *Phys. Rev. B* **11**, 619 (1975).
- [22] H. Grassi, A. Brau, and J.P. Farges, Heat Pulse Diffusion in  $\text{TEA}(\text{TCNQ})_2$ , *Phys. Stat. Sol. (b)* **112**, 633 (1982).
- [23] K. Torizuki, H. Tajima, and T. Yamamoto, Thermal conductivity of  $(\text{DMe-DCNQI})_2\text{Li}_{1-x}\text{Cu}_x$  ( $0 \leq x \leq 0.14$ ): Phonon propagation and the spin-Peierls lattice distortion, *Phys. Rev. B* **71**, 193101 (2005).
- [24] From vibrating reed measurements, we estimate the Young’s modulus velocity to be  $1.2 \pm 0.4$  km/s. [D. Ferguson and J.W. Brill, unpublished results.]
- [25] A. Eggeman, S. Illig, A. Troisi, H. Siiringhaus, and P.A. Midgley, Measurement of molecular motion in organic semiconductors by thermal diffuse electron scattering, *Nature Materials* **12**, 1045 (2013).
- [26] N. Kim, B. Domercq, S. Yoo, A. Christensen, B. Kippelen, and S. Graham, Thermal transport properties of small molecule organic semiconductors, *App. Phys. Lett.* **87**, 241908 (2005).
- [27] E.R. Dobrovinskaya, L.A. Lytvynov, and V. Pishchik, *Sapphire: Material, Manufacturing, Applications* (Springer, 2009, New York).
- [28] F. Rondelez, W. Urbach, and H. Hervet, Origin of Thermal Conductivity Anisotropy in Liquid Crystal Phases, *Phys. Rev. Lett.* **41**, 1058 (1978).
- [29] A.A. Minakov, S.A. Adamovsky, and C. Schick, Advanced two-channel ac calorimetry for simultaneous measurements of complex heat capacity and complex thermal conductivity, *Thermochimica Acta* **304**, 89 (2003).